scientific reports

Check for updates

OPEN

Harnessing Ni–V stabilized Ag/AgCl nanofoam for multifaceted reaction

Manash J. Baruah[1,9], Rajarshi Bayan[2,9], Bitupon Borthakur[3], Shivanee Borpatra Gohain[4], Pallabi Saikia[5], Eramoni Saikia[3], Mamon Dey[6], Rahul Kemprai[7], Young-Bin Park[8], Biraj Das[3]✉ & Mukesh Sharma[7]✉

The demand to address the ongoing environmental pollution has motivated the research community to develop novel methodologies for the degradation of the hazaradous pollutants. This study presents the development of an efficient and resilient Ag/AgCl nanocomposite catalyst supported on $NiVO_x$ surfaces. The catalyst exhibited exceptional stability and photocatalytic performance in the degradation of methylene blue (MB) dye, as well as the reduction of 4-nitrophenol (4-NP) and Cr(VI) ions in presence of $NaBH_4$. A theoretical study has also been performed to investigate the role of silver in enhancing the stability and reactivity of the nanocomposite. This work demonstrates the potential of Ag/AgCl/$NiVO_x$ as a promising material for addressing environmental pollution, offering a stable and effective solution for the degradation of hazardous pollutants.

Keywords Ag/AgCl, $NiVO_x$, Photocatalysis, Environmental remediation, Nanocomposite, Methylene blue, 4-Nitrophenol, Cr(VI) reduction

Environmental pollution has become one of the most pressing challenges facing the world today[1]. Water and soil contamination, particularly by hazardous organic dyes and industrial pollutants, significantly harms ecosystems and human health[2,3]. Among the many pollutants, synthetic dyes from chemical industries and persistent toxic substances like 4-nitrophenol (4-NP) and hexavalent chromium (Cr(VI)) are particularly harmful[4–8]. These pollutants are difficult to degrade using conventional methods, and their persistence in the environment poses severe risks[7]. Photocatalytic degradation has emerged as an effective solution to address these concerns by enabling the breakdown of organic pollutants and the reduction of toxic substances[9,10].

Nanoparticles (NPs), particularly those based on metals such as silver (Ag), have gained significant attention as photocatalysts due to their ability to efficiently absorb solar energy and promote catalytic reactions[11,12]. Noble metal NPs, especially those exhibiting surface plasmon resonance (SPR), are known for their excellent photocatalytic properties, particularly in the degradation of organic pollutants[13,14]. However, challenges such as the recombination of charge carriers and the agglomeration of NPs limit their efficiency and stability during photocatalytic reactions[11]. To overcome these issues, researchers have turned to modifications such as embedding noble metal NPs within metal halides, like AgCl, to enhance their photocatalytic activity and stability[15,16].

Metal oxides, such as vanadium oxide (VO_x), have also attracted significant interest as supports for photocatalysts due to their favourable electronic structures, wide band gaps, and ability to disperse NPs effectively[17,18]. VO_x is particularly advantageous because it is abundant, cost-effective, and non-toxic, making it a promising candidate for photocatalytic applications[19,20]. By combining Ag/AgCl with metal oxide surfaces, such as $NiVO_x$, enhanced photocatalytic performance and improved stability can be achieved[21].

In this study, we focus on the synthesis of a novel Ag/AgCl nanocomposite supported on $NiVO_x$ surfaces for the efficient photocatalytic degradation of methylene blue (MB) dye, reduction of 4-nitrophenol (4-NP),

[1]Department of Chemistry, Devi Charan Baruah Girls' College (D.C.B. Girls' College), Jorhat, Assam 785001, India. [2]Department of Chemistry, Arya Vidyapeeth College, Guwahati, Assam 781016, India. [3]Department of Chemistry, Dakha Devi Rasiwasia College (D. D. R. College), Chabua, Dibrugarh, Assam 786184, India. [4]Department of Chemistry, Dimoria College, Khetri, Kamrup(M), Guwahati, Assam 782403, India. [5]Department of Chemistry, Mangaldai College, Uaphupara, Darrang, Assam 784125, India. [6]Department of Chemistry, Sreenivas Basudev Deorah College (SB Deorah College), Ulubari, Guwahati, Assam 781007, India. [7]Department of Chemistry, Suren Das College, Hajo, Kamrup, Assam 781102, India. [8]Department of Mechanical Engineering, Ulsan National Institute of Science and Technology, UNIST-gil 50, Ulju-gun, Ulsan 44919, Republic of Korea. [9]Manash J. Baruah and Rajarshi Bayan contributed equally to this work. ✉email: birajdaschm@gmail.com; mcotton233@gmail.com

and Cr(VI) ions in presence of $NaBH_4$. This approach offers a promising solution for the degradation of environmental pollutants while maintaining high catalytic stability over multiple cycles.

Experimental section

Material used

Vanadium trichloride (VCl_3) and nickel chloride ($NiCl_2$) were purchased from E-Merck. Silver nitrate ($AgNO_3$), MB dye and $K_2Cr_2O_7$ were brought from Sigma Aldrich. Sodium hydroxide (NaOH) was procured from E-Merck. 4-Nitrophenol and sodium borohydride ($NaBH_4$) were purchased from E-Merck.

Synthesis of Ag-doped $NiVO_x$ material

In a round bottom flask (RBF), 4 mmol of $NiCl_2$ was dissolved in 10 mL of water, and subsequently, 4 mmol of NaOH was introduced into the solution. The resulting mixture underwent stirring for a duration of 2 h to ensure the complete precipitation of nickel hydroxide, $Ni(OH)_2$. Following precipitation, the formed $Ni(OH)_2$ precipitate underwent multiple washings. After this, 4 mmol of VCl_3 was combined with the $Ni(OH)_2$, and the reaction mixture was ground for a period of 24 h. To this mixture, a $AgNO_3$ solution (0.2 mmol) was once again introduced, and the entire mixture was stirred for an additional 6 h. The resulting material was then washed with distilled water and subsequently dried in an oven at 120 °C. The schematic route for the synthesis of Ag-doped $NiVO_x$ material is shown in Scheme 1.

Procedure for the photocatalytic degradation of MB dye with Ag/AgCl/$NiVO_x$ nanocatalyst

The degradation procedure of MB dye was initiated by using a standard solution of MB having a molar concentration of 1×10^{-6} M in an open atmosphere under sunlight exposure. The reaction was started with 50 mL of that solution, then proceeded with the addition of 20 mg of the synthesized Ag/AgCl/$NiVO_x$ catalyst. Before the photocatalytic reaction, the reaction was left in the dark for 1 h to accomplish the adsorption–desorption equilibria, and after 1 h the reaction mixture was subjected to sunlight (average intensity 500–600 W/m^2) for about ~ 6 min. The reaction progress was monitored through UV–vis spectrophotometric analysis by collecting the sample from the reaction vessel at an interval of 3 min.

Procedure for the reduction of 4-NP to 4-AP with Ag/AgCl/$NiVO_x$ nanocatalyst

In a representative procedure, a 0.10 mM standard solution of 4-NP was prepared for the reduction process. Correspondingly, a $NaBH_4$ solution was made by dissolving 50 mg of $NaBH_4$ in 15 mL of water. The reduction began by adding 20 mL of the 4-NP solution into a 50 mL RBF that contained 20 mg of the synthesized Ag/AgCl/$NiVO_x$ nanocatalyst. Subsequently, 500 µL of the $NaBH_4$ solution was gradually introduced. The reaction was conducted under continuous stirring, and the progress was monitored using UV–vis spectroscopy. The reduction of 4-NP was carried out at room temperature (~ 25 °C).

Procedure for the reduction of Cr(VI) to Cr(III) with Ag/AgCl/$NiVO_x$ nanocatalyst

To start the reduction of Cr(VI), 20 mL of a 0.001 N $K_2Cr_2O_7$ solution was placed into a 50 mL RBF, and 20 mg of the synthesized Ag/AgCl/$NiVO_x$ nanocatalyst was added. Following this, 500 µL of $NaBH_4$ solution was slowly introduced into the mixture while continuously stirring. The reaction's progress was tracked using a UV–vis spectrophotometer over the wavelength range of 200–600 nm. This reduction process was carried out at room temperature (~ 25 °C).

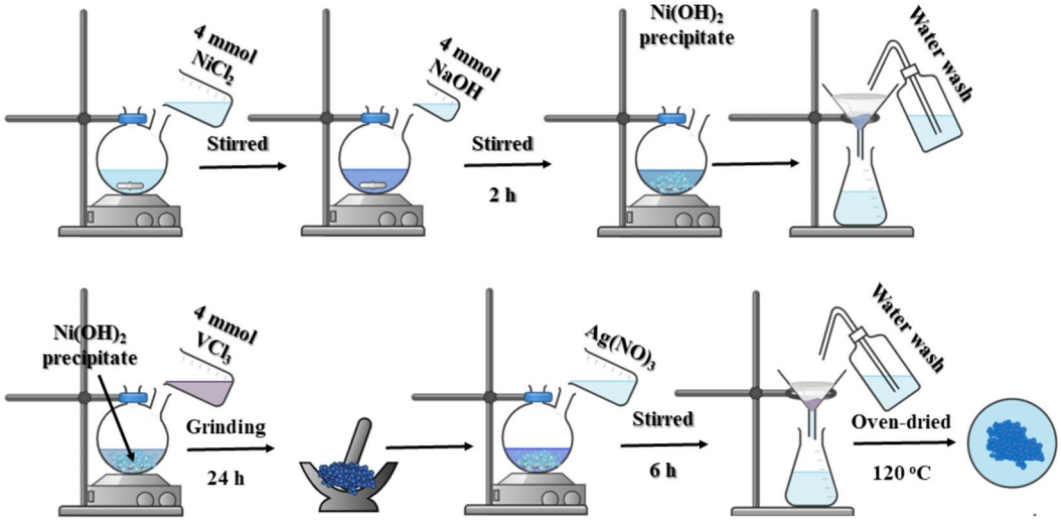

Scheme 1. Schematic diagram for the synthesis of Ag/AgCl/$NiVO_x$.

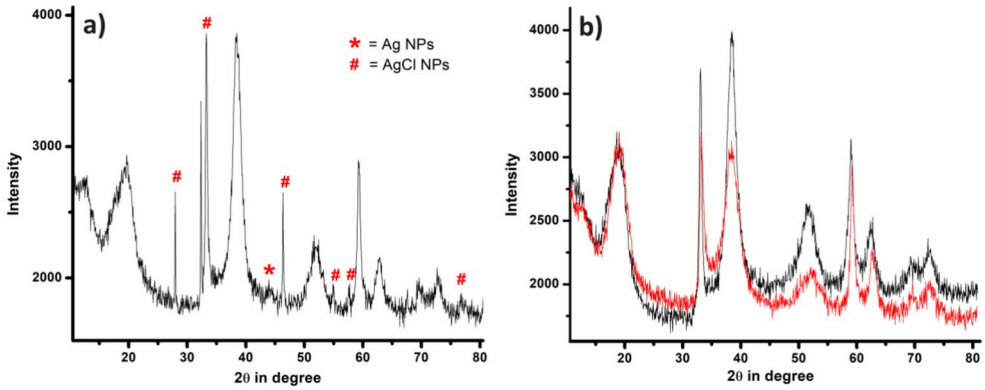

Fig. 1. XRD pattern of (**a**) Ag/AgCl/$NiVO_x$ nanocatalyst and (**b**) $Ni(OH)_2$ (black line) and $NiVO_x$ (red line).

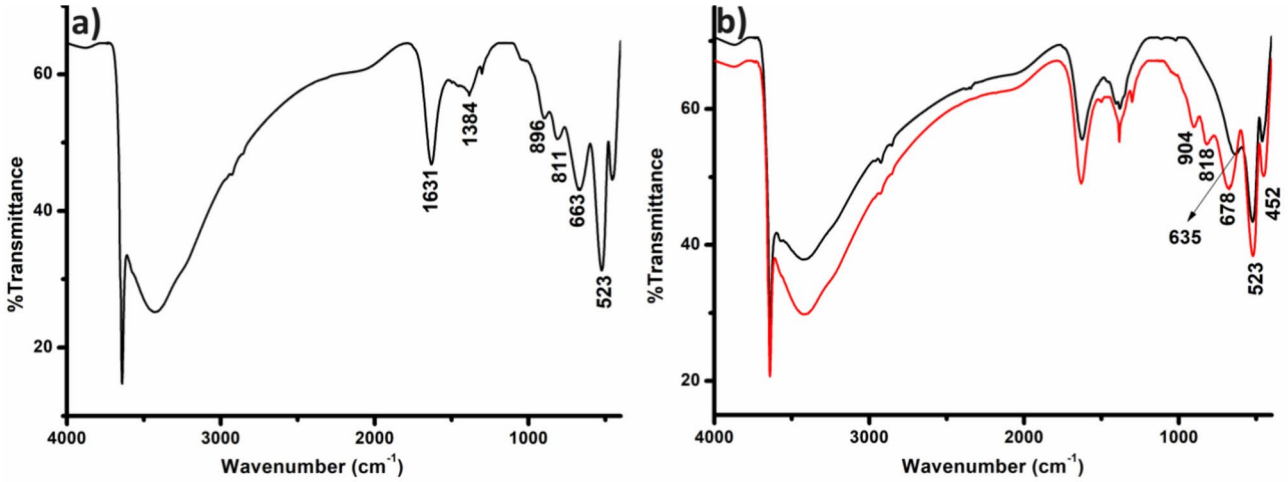

Fig. 2. FTIR spectra of (**a**) Ag/AgCl/$NiVO_x$ nanocatalyst and (**b**) $Ni(OH)_2$ (black line) and $NiVO_x$ (red line).

Results and discussion

Characterization of the synthesized Ag/AgCl/$NiVO_x$ nanocatalyst

After the synthesis, the material was well-characterized by different spectrochemical and physicochemical analyses. The X-ray diffraction (XRD) pattern of the Ag-doped NiV material indicated the presence of peaks at 2θ values of 28.09°, 32.2°, 46.2°, 54.9°, 57.7°, and 76.7°, which were associated with the (111), (200), (220), (311), (222), and (420) planes of AgCl NPs, along with a peak at ~ 44° corresponding to Ag NPs, Fig. 1a[22]. Additionally, the peaks at 2θ values of 38° and 63.5° for Ag NPs coincided with the NiV peaks[23]. To further confirm the synthesis of bimetallic NiV, the XRD pattern of the neat $Ni(OH)_2$ and the V-doped $Ni(OH)_2$ were also recorded as shown in Fig. 1b (black line). The XRD analysis reveals the presence of peaks at 2θ values of 12°, 18.1° (001), 33° (100), 38.5° (101), 51.7° (102), 59° (110), 62.5° (111), 69.2°, and 72.5° corresponding to $Ni(OH)_2$[24]. Post-formation of the $NiVO_x$ bimetallic composite, alterations in peak intensity at 2θ of 33° and 38.5° indicated the formation of bimetallic materials, Fig. 1b (red line)[23]. Esparza and colleagues synthesized AgPd bimetallic material, observing that as the Pd content increased, XRD patterns shifted gradually to larger angles, indicating solid solution formation with alloyed nature or due to alloyed phase formation[25]. Consistent alterations in peak intensities were observed, aligning with our earlier study on catalysts Pd–NiO–Y and Pd–CuO–Y synthesized through the same methodology indicating the bimetallic formation[26–28].

Further characterization of the Ag/AgCl/$NiVO_x$ nanocatalyst was conducted using Fourier Transform Infrared (FTIR) analysis. In the FTIR spectra, the presence of V–O and V–O–V vibrational bands of vanadium oxide was confirmed with peaks at 896 and 811 cm^{-1}, respectively (Fig. 2a)[29]. The observed shift in bands from 635 cm^{-1} (black line) to 678 cm^{-1} (red line) indicated the interaction between Ni and V, Fig. 2b[30]. The FTIR spectra, illustrated in the accompanying figure, revealed a prominent absorption peak at 523 cm^{-1}, corresponding to Ni–O–H bending and Ni–O stretching vibrations, Fig. 2b[31]. The bending vibration associated with the absorbed H_2O molecule was detected at 1622 cm^{-1}. Stretching vibration bands of non hydrogen-bonded hydroxyl groups were evident at 3641 cm^{-1}[31]. Additionally, a broad band representing H_2O molecules in the $Ni(OH)_2$ material was identified at 3429 cm^{-1}, Fig. 2b[31].

The TEM analysis was conducted to examine the surface morphology of the synthesized material, and the results are presented in the accompanying Fig. 3. The TEM images reveal a structure resembling a nanofoam, with Ag NPs distributed in the 20–30 nm range, as depicted in Fig. 3a,b. Furthermore, the lattice fringe pattern of the particles displays a d-spacing of around 0.22 nm, characteristic of the (111) plane of Ag NPs, Fig. 3c[32]. The rings observed in the selected area diffraction pattern (SAED) align with the identified fringes and XRD pattern, Fig. 3d.

In the diffuse reflectance spectra (DRS) of $Ni(OH)_2$, peaks were observed at 392 nm and 683 nm, corresponding to the $^3T_{1g}$ (F) $\leftarrow {}^3A_{2g}$ and $^3T_{1g}$ (P) $\leftarrow {}^3A_{2g}$ transitions, respectively, Fig. 4a (black line)[33]. The transition at 246 nm was postulated as a charge transfer transition[33,34]. In the case of NiV bimetallic nanocomposites, a transition at 339 nm was identified, attributed to VO_x, Fig. 4a (red line)[35]. The DRS spectra of Ag/AgCl/$NiVO_x$ nanocomposite displayed a broad band above 500 nm, indicative of small particle size across the visible range, Fig. 4a (blue line). The nanocomposite material exhibited a band gap of 2.01 eV, suggesting its potential suitability as a photocatalyst in the visible range of the solar spectrum towards various photocatalytic reactions, Fig. 4b.

Further, the oxidation states of all the elements were predicted through the X-ray photoelectron spectroscopic (XPS) analysis, Fig. 5a–f. The XPS analysis of the nanocatalyst revealed peaks at 854.9 eV for Ni $2p_{3/2}$ and a satellite peak at 860.7 eV, Fig. 5a. The Ni $2p_{1/2}$ peaks were observed at 872.5 eV with a satellite peak at 877.9 eV indicating the presence of Ni in the + 2 state[36]. The Ni $2p_{3/2}$ peak was deconvoluted into three subpeaks at 854.5 eV, 855.7 eV, and 860.7 eV, as indicated by the multiplet-split[26]. The deconvoluted V 2p XPS spectrum showed the signal for V(IV) at 516.5 eV and 523.9 eV (Fig. 5b)[37]. However, the presence of a V–O peak was evident at 530.2 eV from both V 2p and O 1s XPS spectra (Fig. 5b,c)[38]. The XPS spectrum of Ag exposed the presence of Ag^+ ions in the material having Ag $3d_{5/2}$ and Ag $3d_{3/2}$ values at 367.2 eV and 373.2 eV, respectively (Fig. 5d). The XPS spectrum of Cl 2p as shown in Fig. 5e represented two peaks at 197.9 eV for Cl $2p_{3/2}$ and 199.5 eV for Cl $2p_{1/2}$[39]. Furthermore, the presence of the Cl 2p doublet with a separation of 1.6 eV was attributed to inorganic Cl^- ions[40]. All the XPS peaks were fitted with respect to C 1s having a binding energy of 284.0 eV, Fig. 5f.

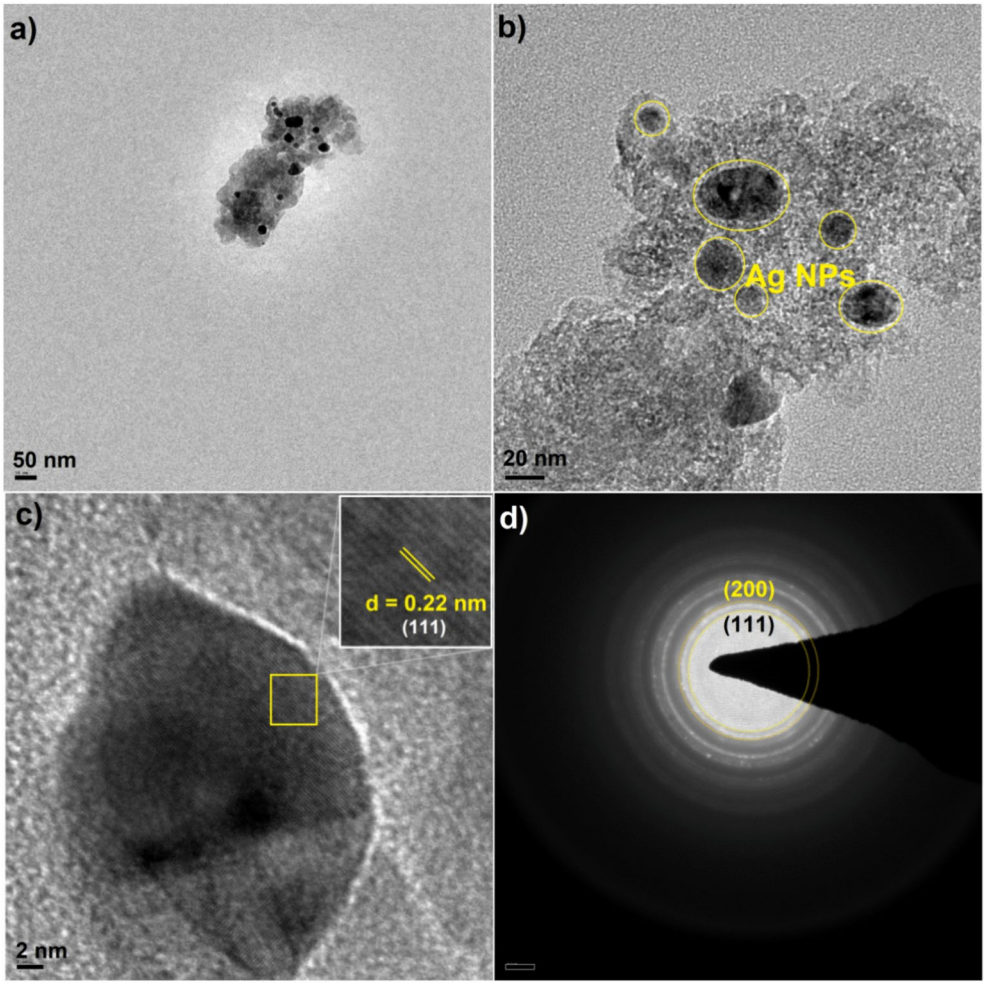

Fig. 3. (**a**–**c**) TEM images of the synthesized Ag/AgCl/$NiVO_x$ nanocatalyst with different magnification, (**d**) SAED pattern.

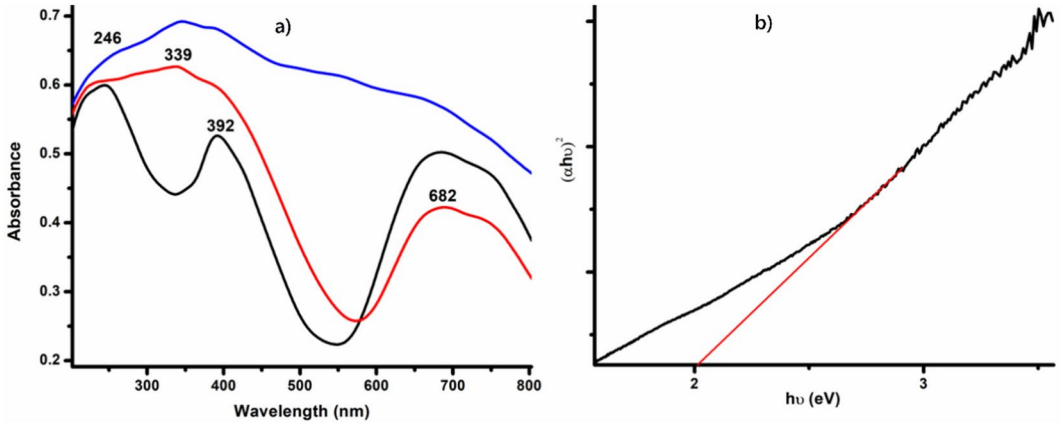

Fig. 4. (**a**) DRS spectra of Ag/AgCl/$NiVO_x$ nanocatalyst (blue line), $Ni(OH)_2$ (black line) and $NiVO_x$ (red line), (**b**) Tauc plot of Ag/AgCl/$NiVO_x$ nanocatalyst.

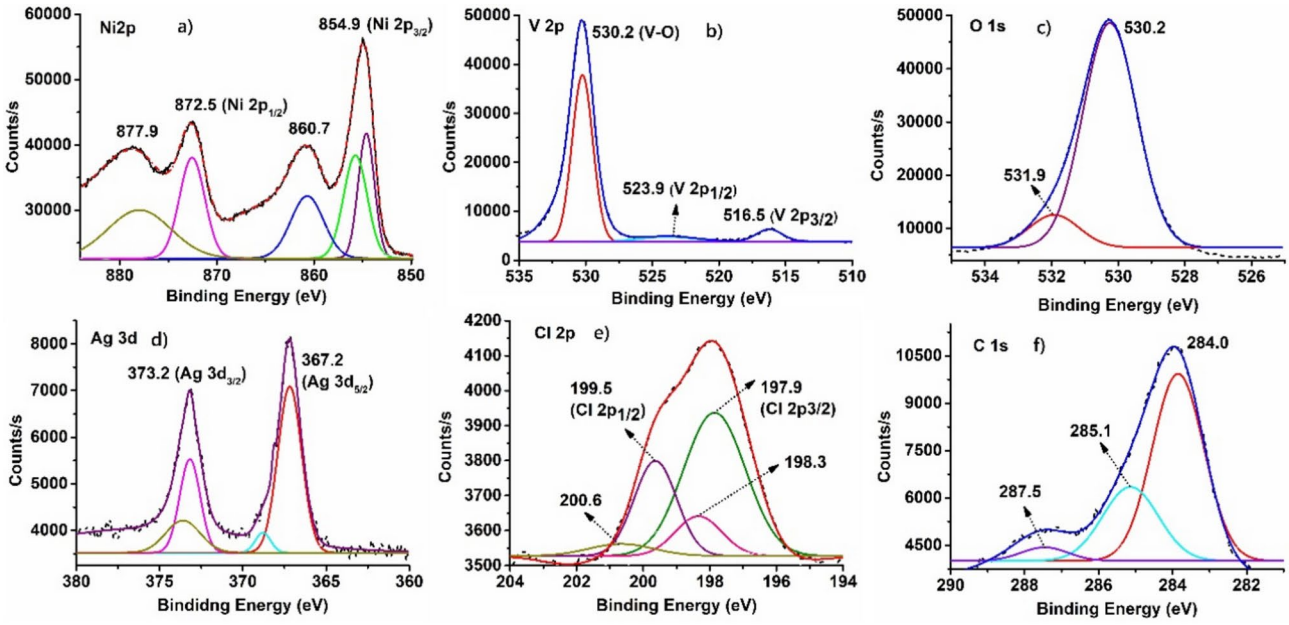

Fig. 5. XPS of (**a**) Ni 2p, (**b**) V 2p, (**c**) O 1s, (**d**) Ag 3d, (**e**) Cl 2p, and (**f**) C 1s in Ag/AgCl/$NiVO_x$ nanocatalyst.

Probable mechanism for the synthesis of Ag/AgCl/$NiVO_x$ nanocatalyst

A plausible mechanism detailing the generation of the Ag/AgCl/$NiVO_x$ nanocatalyst was proposed based on evidence derived from the conducted characterization as shown in Scheme 2. Initially, the mixing of Ni(II) salt with NaOH precipitated a $Ni(OH)_2$ matrix, depicted in **Step 1** and **Step 2**. Subsequent introduction of V(III) ions (**Step 3**) facilitated the exchange of Ni(II) sites with V(III) ions, followed by air oxidation to yield V(IV) ions, thus creating the $NiVO_x$ matrix. This transformation was corroborated by the presence of V–O peaks in the FT-IR spectra and the identification of V(IV) signals in the XPS analysis. The final incorporation of Ag(I) ions culminated in the formation of the Ag/AgCl/$NiVO_x$ catalyst, elucidated in **Step 4**. Notably, the designed $NiVO_x$ matrix served to stabilize the Ag/AgCl NPs on its surface. Additionally, the introduction of vanadium might induces defects within the $Ni(OH)_2$ matrix, thereby serving as supplementary active sites that facilitate enhanced electron transfer crucial for the photocatalytic process.

Catalytic study of Ag/AgCl/$NiVO_x$ nanocatalyst

Degradation profile of MB Dye

Nanomaterials comprising Ag/AgCl NPs on metal oxide support like TiO_2, WO_3, VO_x, ZnO, etc. are well known to be behaving as very efficient photocatalysts for environmental remediation[41–43]. Therefore, looking into these efficacies, we attempted to examine the photocatalytic ability of the synthesized material concerning MB dye degradation.

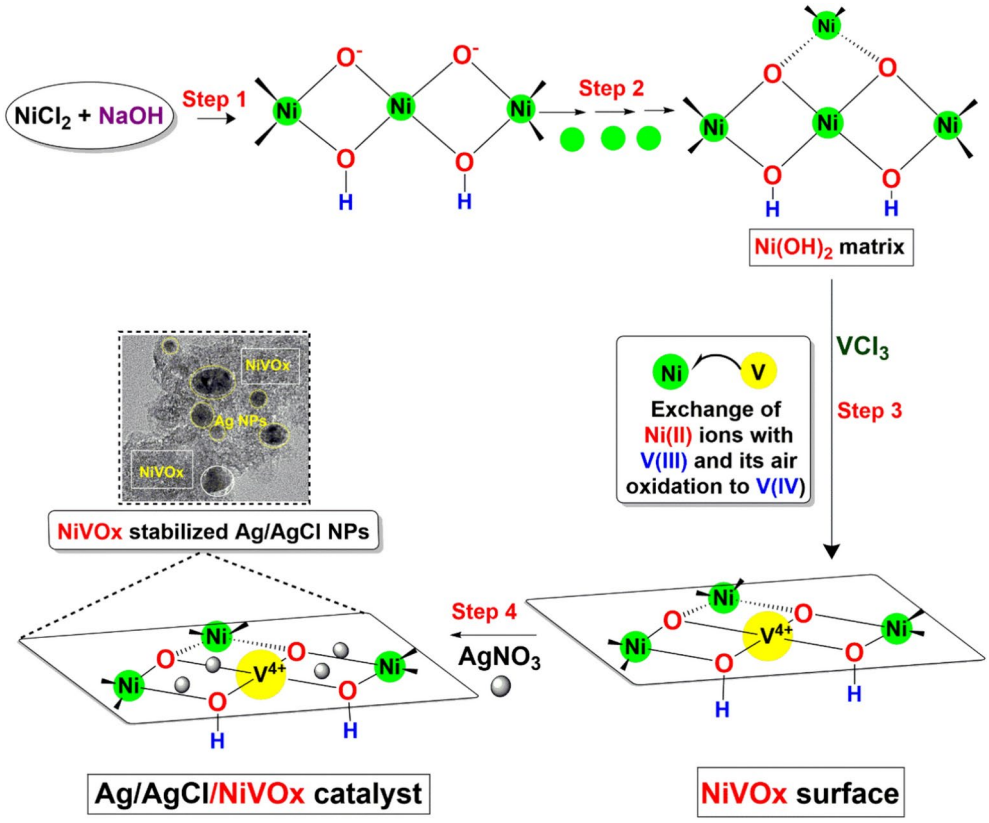

Scheme 2. Probable mechanistic route for the Ag/AgCl/$NiVO_x$ nanocatalyst.

To do so, initially, a standard solution of MB (1×10^{-6} M) was prepared in 500 mL distilled water. From that solution, 50 mL was taken out to set up the reaction followed by the addition of 5 mg of the Ag/AgCl/$NiVO_x$ nanocatalyst. As previously stated, the reaction was kept in the dark for 1 h before the photocatalytic reaction, and after 1 h the reaction mixture was exposed to sunlight. The progress of the reaction was monitored under UV–Vis spectroscopic analysis by collecting the samples at an interval of 3 min. In the presence of 5 mg Ag/AgCl/$NiVO_x$ the absorbance value of the characteristic peak of MB at ~ 665 nm gradually diminished with increasing the time of exposure. The complete decolorization of the MB sample was observed within an interval of 18–20 min of the sunlight experience, Fig. 6a. It is noteworthy that the amount of the catalyst in a catalytic reaction plays a vital role in determining the rate of the catalytic reaction[38,44,45]. Therefore, to study the impact of the catalyst herein the amount was varied from 5 to 20 mg and the UV–Vis spectra were recorded similarly. After using 10 mg of the synthesized catalyst in the reaction vessel, it was noticed that the MB sample decolourized within ~ 12 min, Fig. 6b. The same reaction was also optimized by using 15 mg and 20 mg of the catalyst. It was observed that the complete bleaching occurs at an interval of 9 min and 6 min while using 15 mg and 20 mg of Ag/AgCl/$NiVO_x$, respectively (Fig. 6c,d). The catalyst amount was further exceeded upto 25 mg, but no significant improvement was observed. Therefore, it can be said that 20 mg of the synthesized Ag/AgCl/$NiVO_x$ nanocatalyst is sufficient enough to degrade the standard solution of MB dye within 6 min. To find out whether the visible or UV range affects the photocatalytic oxidation process, we also looked at the identical reaction under a UV lamp. However, for 3 h, we saw no change in dye colour under the UV light irradiation. This further substantiates that the visible spectrum of sunlight plays a crucial role in facilitating the photocatalytic oxidation process. Following the same reaction condition, a dark experiment was also carried out. The reaction setup was placed in a dark chamber and its response was monitored at night. However, no decolourization of the MB sample as well as no change in the UV–Vis absorbances of the sample indicated the true assistance of the visible light source in the catalytic progress. Therefore, we can say that the synthesized nanocomposite material can be efficiently employed as an excellent visible-light-driven photocatalyst.

Mechanism for the photodegradation of MB dye

To investigate the mechanism of the reaction and determine the involvement of holes (h^+) or electrons (e^-), specific scavenging agents were employed. Silver nitrate ($AgNO_3$) was used as an electron scavenger, while ammonium oxalate served as a hole scavenger[46]. The reaction was conducted separately under optimal conditions, once with $AgNO_3$ and once with ammonium oxalate. In both cases, the reaction completion time was notably prolonged. This observation confirmed the involvement of both holes and electrons in the photocatalytic degradation of MB dye, aligning with the proposed reaction mechanism.

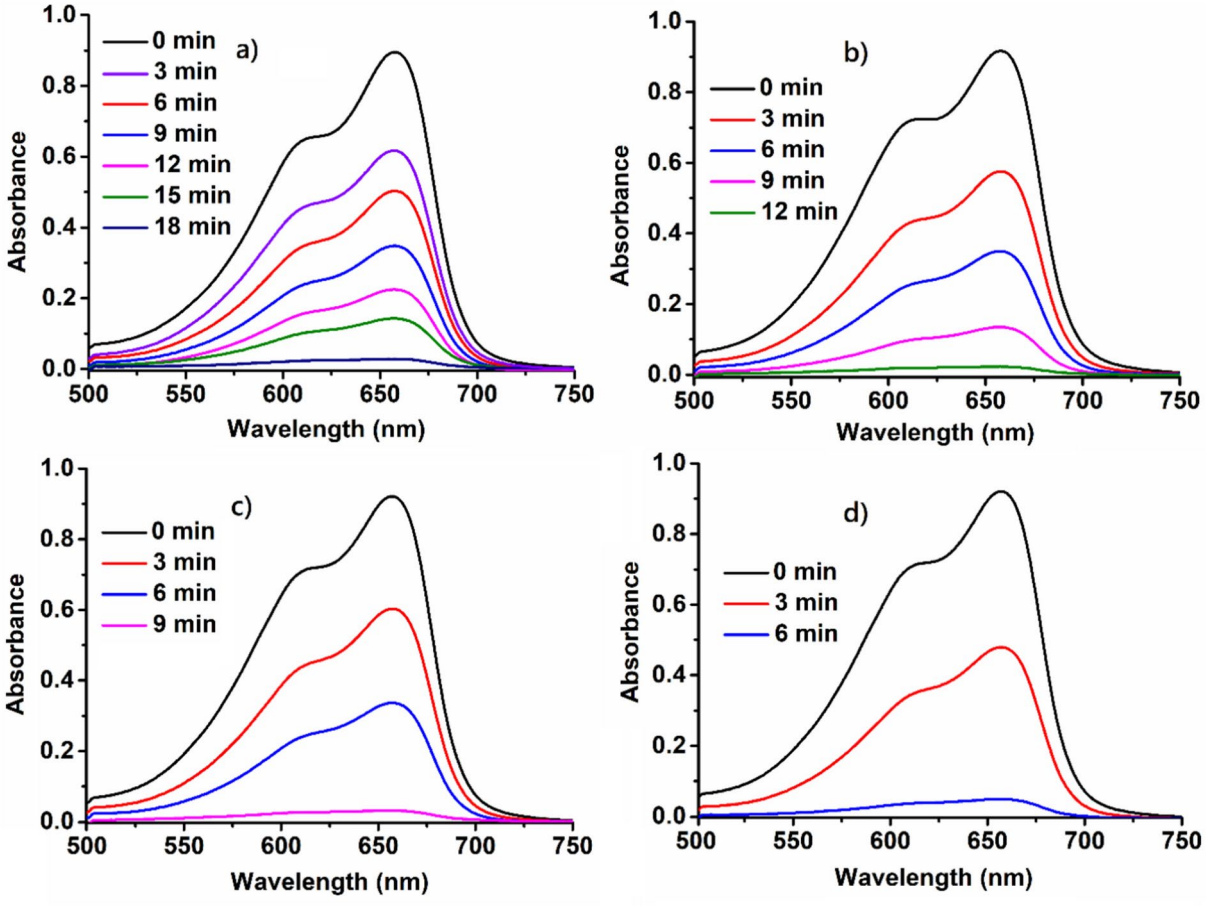

Fig. 6. Photocatalytic degradation of MB dye using (**a**) 5 mg, (**b**) 10 mg, (**c**) 15 mg, and (**d**) 20 mg of Ag/AgCl/$NiVO_x$ nanocatalyst.

Upon exposure to visible light, electrons are excited to the conduction bands (CB) of Ag/$NiVO_x$ and Ag/AgCl, leaving holes in their valence bands (VB). Electrons in the CB of Ag/$NiVO_x$ can migrate to the CB of Ag/AgCl, while holes can move from the VB of Ag/AgCl to the VB of Ag/$NiVO_x$. However, MB degradation utilizing Ag-based material as a catalyst is significantly influenced by the Ag plasmon resonance. The SPR effect can produce excited electron–hole pairs that can result in the production of $O_2^{\cdot-}$ species[47]. This efficient charge transfer, facilitated by strong interfacial coupling, allows electrons to react with O_2, forming redox-active $O_2^{\cdot-}$ species that further oxidize MB[48,49]. The overall mechanistic pathways for the Ag/AgCl/$NiVO_x$ catalyzed degradation of MB are depicted in Scheme 3. Similar mechanistic profile for the degradation of triphenylmethane was also reported by Wang et al.[50].

Reduction of 4-NP to 4-AP

To evaluate the catalytic performance of the synthesized nanocatalyst, we carried out a reduction reaction that converts 4-NP to 4-AP using $NaBH_4$ as the reducing agent. This reaction is commonly used to assess the catalytic effectiveness of various nanocatalysts. The progress of the reaction at room temperature was monitored using UV–Vis spectrophotometry. In this procedure, as described in the experimental Section, a solution of 3 mL of aqueous 4-NP (0.10 mM) was placed into a quartz cuvette for UV–Vis analysis. The initial UV–Vis absorption spectrum displayed a characteristic peak at 400 nm for the 4-nitrophenolate ion (Fig. 7a, red). After adding 20 mg of the Ag/AgCl/$NiVO_x$ nanocatalyst, a noticeable decrease in the intensity of this peak was observed over time, along with the appearance of a new absorption peak at 298 nm (Fig. 7b) within 4 min.

A characteristic peak at 315 nm was initially observed while recording the UV–visible absorption spectrum of a 0.10 mM solution of 4-NP. Upon mixing a 500 µL of $NaBH_4$ solution, the formation of the corresponding 4-nitrophenolate ion was observed with its characteristic peak at 400 nm. After adding $NaBH_4$, the reaction mixture was stirred for 10 min without the nanocatalyst, and the UV–Vis absorption spectra showed no evidence of the 4-AP product. However, when 20 mg of the synthesized Ag/AgCl/$NiVO_x$ was introduced into the reaction mixture, a decrease in the peak intensity at 400 nm was observed, accompanied by a colour change in the solution, Fig. 7b. Successive UV–Vis spectra recordings over time demonstrated the appearance of a new peak at 298 nm, indicative of 4-AP formation, as depicted in Fig. 7b (black). Moreover, a control experiment involving the mixture of 4-NP with Ag/AgCl/$NiVO_x$ in the absence of $NaBH_4$ showed no evidence of reduction, thereby underscoring the catalytic efficacy of the nanocatalyst in facilitating the reduction process. To further

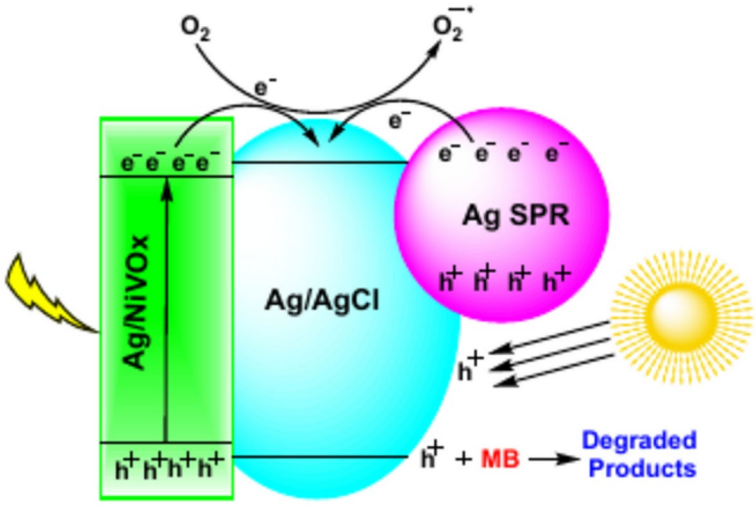

Scheme 3. Plausible mechanism for the visible light assisted MB degradation catalysed by Ag/AgCl/$NiVO_x$.

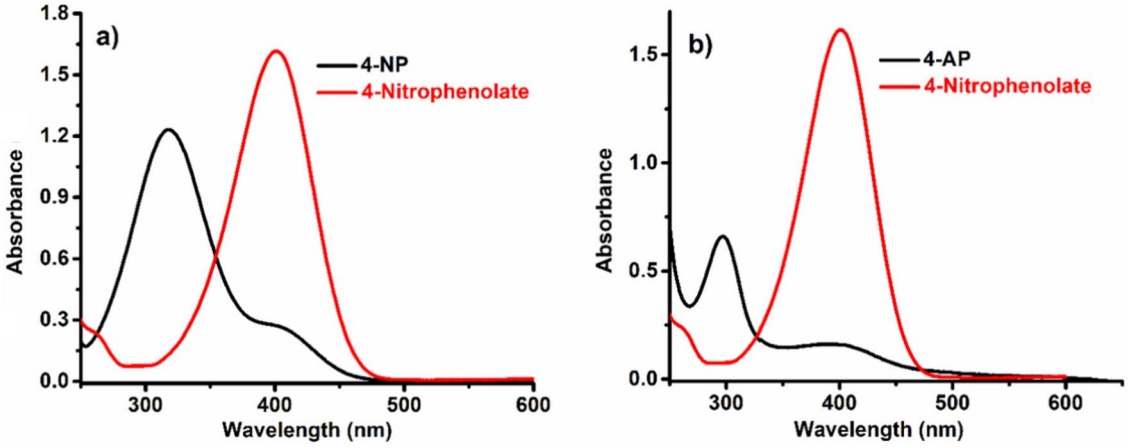

Fig. 7. (**a**) UV–visible absorption spectra of 4-NP and 4-Nitrophenolate, (**b**) UV–visible absorption spectra of 4-AP after addition of Ag/AgCl/$NiVO_x$ nanocatalyst.

confirm the successful formation of 4-AP as the reduced product, the reaction was further analysed using LC–MS. The corresponding LC–MS data illustrating the reaction progress is provided in the Supporting Information (SI), Fig. S1.

Reduction of Cr(VI) to Cr(III)

The reduction of Cr(VI) to Cr(III) was accomplished by adding 500 µL of $NaBH_4$ to a 10 mL $K_2Cr_2O_7$ solution containing 20 mg of the synthesized Ag/AgCl/$NiVO_x$ nanocatalyst. In the UV–Vis spectra, the $K_2Cr_2O_7$ exhibited distinct absorption peaks at 273 nm and 375 nm, corresponding to ligand-to-metal ($O_2 \rightarrow Cr$) charge transfer transitions (Fig. 8a, blue). Spectroscopic analysis indicated a progressive decrease in the absorption peak at 373 nm, marking the reduction process (Fig. 8a, red). This reduction was visually evidenced by the transition of the solution from yellow to colourless, confirming the formation of Cr(III) ions. Initially, neither the Ag/AgCl/$NiVO_x$ nanocatalyst alone nor $NaBH_4$ alone influenced these absorption bands. However, upon the combined introduction of Ag/AgCl/$NiVO_x$ and $NaBH_4$, the absorption bands decreased within 5 min, indicating a rapid reduction of Cr(VI) to Cr(III) (Fig. 8a, red and green). To understand the role of the nanocatalyst, the reaction was carried out using only neat $NaBH_4$, without the presence of Ag/AgCl/$NiVO_x$. It was observed that, in the absence of the catalyst, the reduction reaction did not proceed effectively, Fig. 8b. Furthermore, in the presence of $NaBH_4$ alone, a slight shift in the UV peaks of Cr(VI) was noted, Fig. 8b. This clearly highlights the crucial role of the synthesized Ag/AgCl/$NiVO_x$ nanocatalyst in facilitating the efficient reduction of Cr(VI) to Cr(III). The formation of Cr(III) species was further investigated through XPS analysis and the corresponding XPS spectrum was provided in SI, Fig. S2.

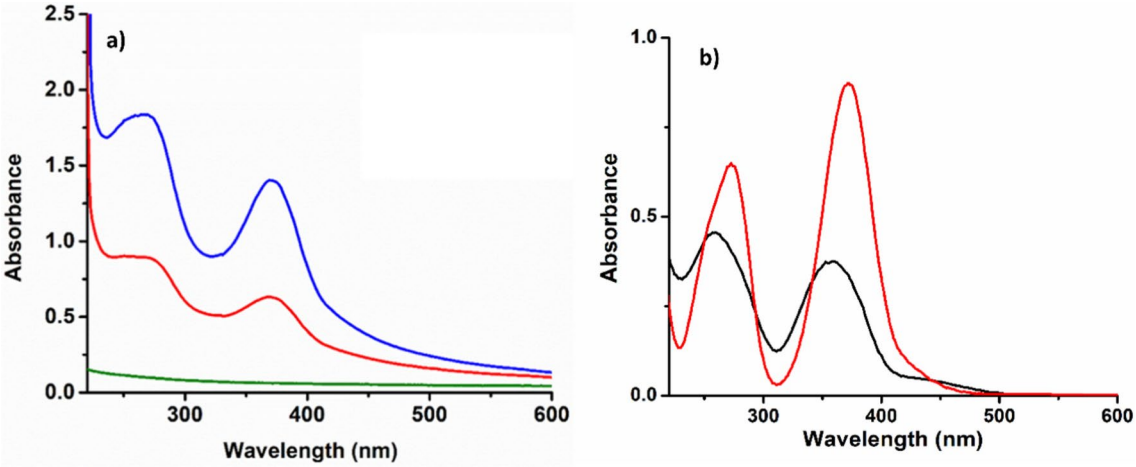

Fig. 8. (**a**) Reduction profile of Cr(VI) using Ag/AgCl/$NiVO_x$ nanocatalyst, (**b**) UV–Vis spectrum of neat Cr(VI) species (black), Cr(VI) + $NaBH_4$ (red).

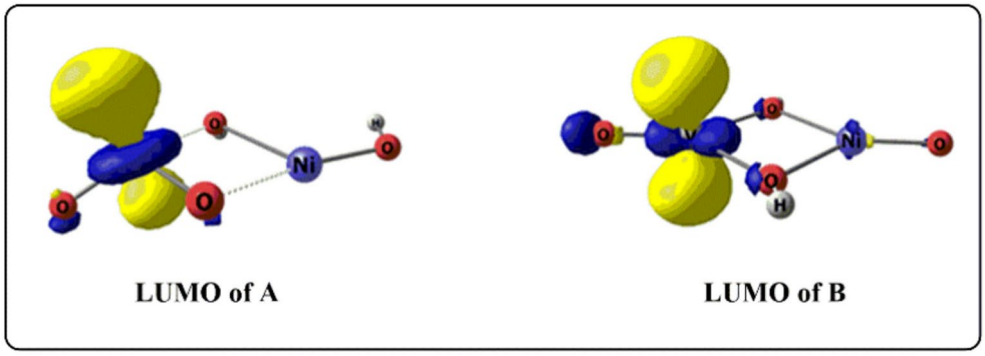

Fig. 9. Lowest Unoccupied Molecular Orbital (LUMO) of **A** and **B**.

Computational analysis of bimetallic isomer stability and reactivity: silver enhanced coordination with vanadium

A theoretical study has been conducted to observe the role of silver support in enhancing reactivity through coordination with the vanadium centre. We have considered two possible isomers (**A** & **B**, Fig. 9) for the bimetallic site of the catalyst. Energy considerations indicate that the isomer **A** is more stable than **B** by almost 42 kcal. An inspection of the molecular orbitals indicates that the Lowest Unoccupied Molecular Orbital (LUMO) of both **A** and **B** (Fig. 9) are highly concentrated on the vanadium centre thereby suggesting that the primary interaction of the silver support will be with the vanadium atom. Interestingly, optimization of the molecules incorporating silver support shows that the silver atom has dominant coordination with the vanadium centre in both the isomers.

In order to gauge the reactivity of the catalyst we have computed the HOMO – LUMO gaps (ΔE_{H-L}) for all the molecules. Between **A** and **B**, the ΔE_{H-L} for **A** (~ 5.2 eV) is found to be lower than that of **B** (~ 5.9 eV) indicating the higher reactivity of the former than the later. Therefore, isomer **A** can be anticipated as the most probable structure for the bimetallic catalyst on the basis of its higher thermodynamic stability and reactivity. Further, incorporation of the silver support significantly reduces the ΔE_{H-L} values for both the isomers thereby suggesting increasing reactivity which is akin to the experimental findings. Figure 10 shows the reduction in ΔE_{H-L} values for isomer **A**.

Recyclability test of the catalyst

The reusability of catalysts is one of the crucial aspects in heterogeneous catalytic transformations. An ideal heterogeneous catalyst can be used multiple times in its specific catalytic conversion without losing its heterogeneous nature. To assess the recyclability of Ag/AgCl/$NiVO_x$, the photocatalytic degradation of MB dye was selected as the test reaction. We used the hot filtering procedure to see whether the reaction continued with the filtrate in order to judge the heterogeneity of the catalyst. However, the colour of the MB dye remained intact after prolonged exposure to the sunlight on the filtrate of the reaction mixture obtained from the hot filtration method. This suggested that the heterogeneity of the catalyst was preserved effectively in the reaction medium. After successfully degrading the 1st set of MB dye samples under the optimized reaction condition, the Ag/

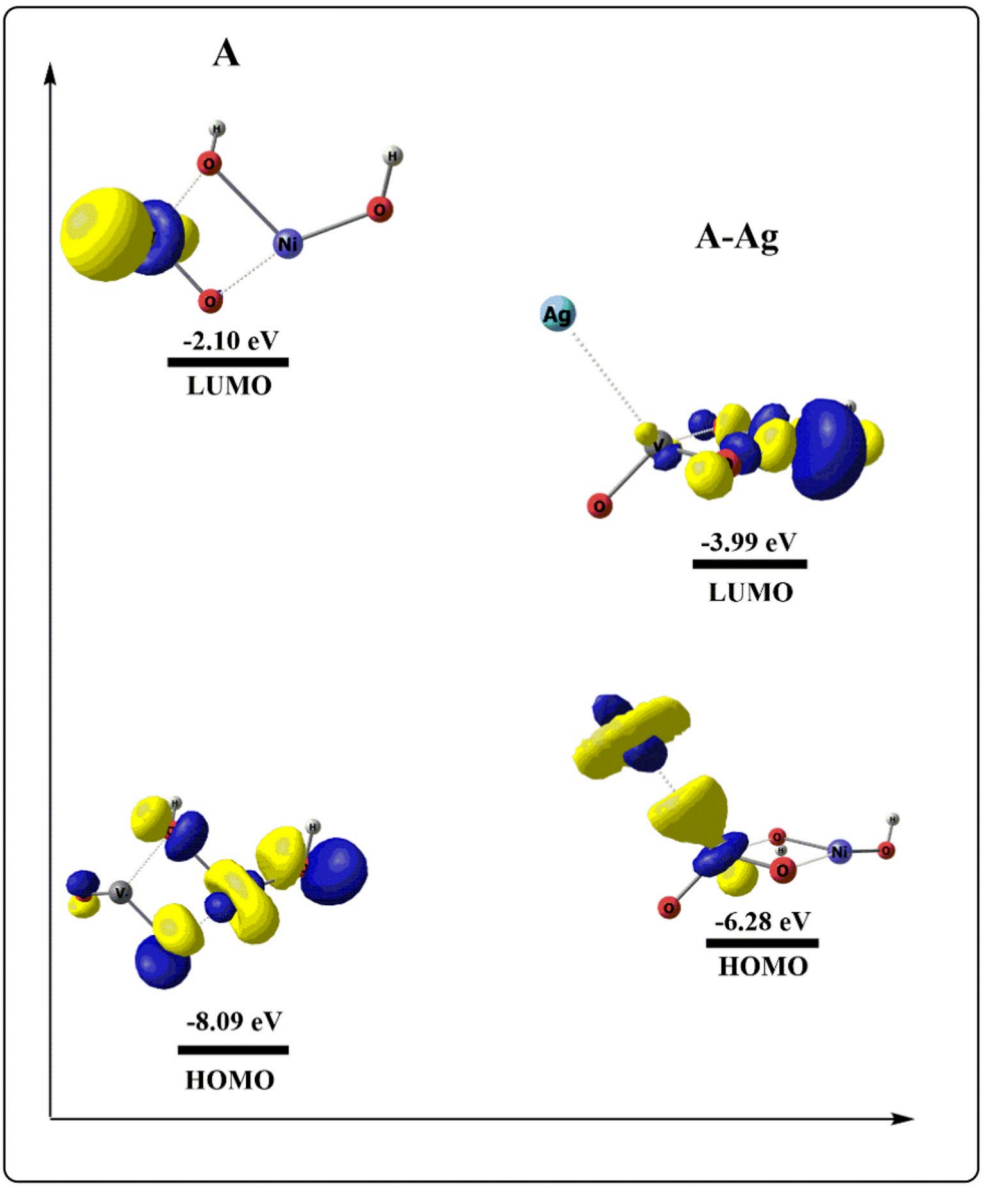

Fig. 10. ΔE_{H-L} values (in eV, not in scale) for isomer **A** and **A**-Ag.

AgCl/$NiVO_x$ catalyst was separated by simple filtration with hot water and washed severely with acetone and distilled water. The recovered catalyst was then dried in an oven at 120 °C for 3–4 h and then employed in the successive catalytic cycle. Fortunately, upto the 9th reaction cycle, the recovered catalyst successfully showed its encouraging status by efficiently decolourizing the standard MB sample within an interval of 6–10 min of the sunlight contact, Fig S3. From the 9th cycle, there occurred a gradual increase in the reaction time of the MB decolourization indicating the dropping in the catalytic activity of the recovered catalyst for the further successive runs. The noteworthy fall in the activity of the reused catalyst may be attributed to the leaching of the active metal content from the catalyst due to the prolonged use of the catalyst in the chemical environment.

Conclusion

In conclusion, this study introduces an efficacious methodology for fabricating a robust photocatalyst, showcasing consistent and exceptional performance. The straightforward synthesis and characterization of an Ag/AgCl nanocomposite on $NiVO_x$ surfaces, a novel approach previously unexplored, resulted in a remarkable degradation rate of hazardous MB dye within an impressively short 5–6-min exposure to sunlight. The same material was also found to be effective in the reduction of 4-NP to 4-AP and Cr(VI) to Cr(III) ion using $NaBH_4$ as a reductant. These discoveries have the potential to significantly advance the development of sustainable and advanced photocatalytic materials, emphasizing improved stability and efficacy in catalyst synthesis for the multifaceted reaction.

Data availability

The authors declare that the data supporting the findings of this study are available within the paper and its Supplementary Information files. Should any raw data files be needed in another format they are available from the corresponding author upon reasonable request.

Received: 29 October 2024; Accepted: 27 February 2025
Published online: 02 July 2025

References

1. Mehndiratta, P., Jain, A., Srivastava, S. & Gupta, N. Environmental pollution and nanotechnology. *Environ. Pollut.* **2**, 49–58 (2013).
2. Long, C. et al. Applications of carbon dots in environmental pollution control: A review. *Chem. Eng. J.* **406**, 126848 (2021).
3. Ma, X., Chai, Y., Li, P. & Wang, B. Metal–organic framework films and their potential applications in environmental pollution control. *Acc. Chem. Res.* **52**, 1461–1470 (2019).
4. Bilal, M., Bagheri, A. R., Bhatt, P. & Chen, S. Environmental occurrence, toxicity concerns, and remediation of recalcitrant nitroaromatic compounds. *J. Environ. Manag.* **291**, 112685 (2021).
5. Nidheesh, P. V. Heterogeneous Fenton catalysts for the abatement of organic pollutants from aqueous solution: A review. *RSC Adv.* **5**, 40552–40577 (2015).
6. Cardoso Juarez, A. O., Ivan Ocampo Lopez, E., Kesarla, M. K. & Bogireddy, N. K. R. Advances in 4-nitrophenol detection and reduction methods and mechanisms: An updated review. *ACS Omega* **9**, 33335–33350 (2024).
7. Farooq, M. et al. Ultra efficient 4-Nitrophenol reduction, dye degradation and Cr(VI) adsorption in the presence of phytochemical synthesized Ag/ZnO nanocomposite: A view towards sustainable chemistry. *Inorg. Chem. Commun.* **136**, 109189 (2022).
8. Barrera-Díaz, C. E., Lugo-Lugo, V. & Bilyeu, B. A review of chemical, electrochemical and biological methods for aqueous Cr(VI) reduction. *J. Hazard. Mater.* **223**, 1–12 (2012).
9. Kaur, K., Badru, R., Singh, P. P. & Kaushal, S. Photodegradation of organic pollutants using heterojunctions: A review. *J. Environ. Chem. Eng.* **8**, 103666 (2020).
10. Gusain, R., Gupta, K., Joshi, P. & Khatri, O. P. Adsorptive removal and photocatalytic degradation of organic pollutants using metal oxides and their composites: A comprehensive review. *Adv. Colloid Interface Sci.* **272**, 102009 (2019).
11. Belessiotis, G. V. & Kontos, A. G. Plasmonic silver (Ag)-based photocatalysts for H_2 production and CO_2 conversion: Review, analysis and perspectives. *Renew. Energy* **195**, 497–515 (2022).
12. Li, G., Yang, C., He, Q. & Liu, J. Ag-based photocatalytic heterostructures: Construction and photocatalytic energy conversion application. *J. Environ. Chem. Eng.* **10**, 107374 (2022).
13. An, C. et al. Plasmonic silver incorporated silver halides for efficient photocatalysis. *J. Mater. Chem. A* **4**, 4336–4352 (2016).
14. Paul, T. K. et al. Mapping the Progress in surface plasmon resonance analysis of phytogenic silver nanoparticles with colorimetric sensing applications. *Chem. Biodivers.* **20**, 202300510 (2023).
15. Nasrollahzadeh, M., Mahmoudi-Gom Yek, S., Motahharifar, N. & Ghafori Gorab, M. Recent developments in the plant-mediated green synthesis of Ag-based nanoparticles for environmental and catalytic applications. *Chem. Rec.* **19**, 2436–2479 (2019).
16. Xue, W. et al. Silver-based semiconductor Z-scheme photocatalytic systems for environmental purification. *J. Hazard. Mater.* **390**, 122128 (2020).
17. Monfort, O. & Petrisková, P. Binary and ternary vanadium oxides: General overview, physical properties, and photochemical processes for environmental applications. *Processes* **9**, 214 (2021).
18. Yu, Y. et al. V_2O_5-based photocatalysts for environmental improvement: Key challenges and advancements. *J. Environ. Chem. Eng.* **11**, 111243 (2023).
19. Li, Y. et al. Research progress of vanadium pentoxide photocatalytic materials. *RSC Adv.* **13**, 22945–22957 (2023).
20. Gonçalves, J. M., da Silva, M. I., Angnes, L. & Araki, K. Vanadium-containing electro and photocatalysts for the oxygen evolution reaction: A review. *J. Mater. Chem. A* **8**, 2171–2206 (2020).
21. Mo, F., Zhou, Q. & He, Y. Nano–Ag: Environmental applications and perspectives. *Sci. Total Environ.* **829**, 154644 (2022).
22. Jing, Y. et al. Synthesis of Ag and AgCl co-doped ZIF-8 hybrid photocatalysts with enhanced photocatalytic activity through a synergistic effect. *RSC Adv.* **10**, 698–704 (2020).
23. Wang, G., Liu, G. & Jin, Z. Interfacial modification to nanflower-like NiV-layered double hydroxide for enhancing supercapacitor performance. *ACS Appl. Nano Mater.* **6**, 8603–8616 (2023).
24. Steimecke, M. et al. Higher-valent nickel oxides with improved oxygen evolution activity and stability in alkaline media prepared by high-temperature treatment of $Ni(OH)_2$. *ACS Catal.* **10**, 3595–3603 (2020).
25. Santoveña-Uribe, A. et al. Synthesis and characterization of AgPd bimetallic nanoparticles as efficient electrocatalysts for oxygen reduction reaction. *Electrocatalysis* **11**, 536–545 (2020).
26. Sharma, M. et al. C-Cl bond activation with Pd(II)–NiO nanoparticles supported on zeolite-Y: The role of charge transfer transition. *Mol. Catal.* **432**, 210–219 (2017).
27. Sharma, M. et al. Pd–NiO-Y/CNT nanofoam: A zeolite-carbon nanotube conjugate exhibiting high durability in methanol oxidation. *Chem. Commun.* **56**, 375–378 (2020).
28. Sharma, M. et al. Pd/Cu-oxide nanoconjugate at zeolite-Y crystallite crafting the mesoporous channels for selective oxidation of benzyl-alcohols. *ACS Appl. Mater. Interfaces* **9**, 35453–35462 (2017).
29. Li, Y. et al. The nature of VO_x structures in HMS supported vanadium catalysts for non-oxidative propane dehydrogenation. *J. Catal.* **413**, 658–667 (2022).
30. George, A. et al. Regeneration study of MB in recycling runs over nickel vanadium oxide by solvent extraction for photocatalytic performance for wastewater treatments. *Environ. Res.* **211**, 112970 (2022).
31. Mozaffari, S. A., Najafi, S. H. M. & Norouzi, Z. Hierarchical NiO@$Ni(OH)_2$ nanoarrays as high-performance supercapacitor electrode material. *Electrochim. Acta* **368**, 137633 (2021).
32. Saad, A. et al. Ag nanoparticles modified crumpled borophene supported Co_3O_4 catalyst showing superior oxygen evolution reaction (OER) performance. *Appl. Catal. B Environ.* **298**, 120529 (2021).
33. Nayak, S. & Parida, K. M. Deciphering Z-scheme charge transfer dynamics in heterostructure NiFe-LDH/N-rGO/g-C_3N_4 nanocomposite for photocatalytic pollutant removal and water splitting reactions. *Sci. Rep.* **9**, 2458 (2019).
34. Yu, J., Hai, Y. & Cheng, B. Enhanced photocatalytic H_2-production activity of TiO_2 by $Ni(OH)_2$ cluster modification. *J. Phys. Chem. C* **115**, 4953–4958 (2011).
35. Li, G. et al. A bimetallic synergistic effect on the atomic scale of defect-enriched NiV-layered double hydroxide nanosheets for electrochemical phenol hydroxylation. *J. Mater. Chem. A* **10**, 6748–6761 (2022).
36. Hoque, N. et al. Impregnating rhodium (0) sites through zeolite-Y templation in a hybrid Rh–Ni catalyst for alcohol electro-oxidation with low CO poisoning. *ACS Appl. Energy Mater.* **5**, 6118–6128 (2022).
37. Sahoo, R., Lee, T. H., Pham, D. T., Luu, T. H. T. & Lee, Y. H. Fast-charging high-energy battery–supercapacitor hybrid: Anodic reduced graphene oxide–vanadium(IV) oxide sheet-on-sheet heterostructure. *ACS Nano* **13**, 10776–10786 (2019).
38. Das, B. et al. Gold nanoparticle supported on mesoporous vanadium oxide for photo-oxidation of 2-naphthol with hydrogen peroxide and aerobic oxidation of benzyl alcohols. *J. Environ. Chem. Eng.* **8**, 104268 (2020).

39. Choi, S. et al. Structural effectiveness of AgCl-decorated Ag nanowires enhancing oxygen reduction. *ACS Sustain. Chem. Eng.* **9**, 7519–7528 (2021).
40. Das, B. et al. Self pH regulated iron(II) catalyst for radical free oxidation of benzyl alcohols. *Appl. Catal. A General* **589**, 117292 (2020).
41. Li, Y. et al. Efficient WO_3 photoanode modified by Pt layer and plasmonic Ag for enhanced charge separation and transfer to promote photoelectrochemical performances. *ACS Sustain. Chem. Eng.* **7**, 12582–12590 (2019).
42. Zhao, H. et al. Self-driven salt-thermal reduction approach for the synthesis of Cu_2O and AgCl–Cu_2O hybrids with superior photocatalytic activity. *ACS Sustain. Chem. Eng.* **9**, 5651–5660 (2021).
43. Yu, X. et al. Efficient visible light photocatalytic antibiotic elimination performance induced by nanostructured Ag/AgCl@Ti^{3+}-TiO_2 mesocrystals. *Chem. Eng. J.* **403**, 126359 (2021).
44. Bhargava, S. S. et al. System design rules for intensifying the electrochemical reduction of CO_2 to CO on Ag nanoparticles. *ChemElectroChem* **7**, 2001–2011 (2020).
45. Baruah, M. J. et al. Fe_2O_3 nanocatalysts supported on zeolite-Y for the selective synthesis of C_2 di-indolyl indolones and isatins. *ACS Appl. Nano Mater.* **5**, 1446–1459 (2022).
46. Baruah, M. J. et al. Chirally modified cobalt-vanadate grafted on battery waste derived layered reduced graphene oxide for enantioselective photooxidation of 2-naphthol: Asymmetric induction through non-covalent interaction. *J. Colloid Interface Sci.* **608**, 1526–1542 (2022).
47. Wang, S. et al. Fabrication of a novel bifunctional material of BiOI/Ag_3VO_4 with high adsorption photocatalysis for efficient treatment of dye wastewater. *Appl. Catal. B Environ.* **168**, 448–457 (2015).
48. Zhang, S. et al. Hybrid 0D–2D nanoheterostructures: In situ growth of amorphous silver silicates dots on g-C_3N_4 nanosheets for full-spectrum photocatalysis. *ACS Appl. Mater. Interfaces* **8**, 35138–35149 (2016).
49. Zhu, X. et al. Novel high-efficiency visible-light responsive $Ag_4(GeO_4)$ photocatalyst. *Catal. Sci. Technol.* **7**, 2318–2324 (2017).
50. Wang, S. et al. Synthesis and characterization of g-C_3N_4/Ag_3VO_4 composites with significantly enhanced visible-light photocatalytic activity for triphenylmethane dye degradation. *Appl. Catal. B Environ.* **144**, 885–892 (2014).

Acknowledgements

MJB, BD, and MS sincerely acknowledge D.C.B. Girls College, Jorhat, D. D. R. College, Chabua, Dibrugarh, and Suren Das College, Hajo, Kamrup, Assam, India for the analytical facilities provided to perform the experimental works. The authors would like to express their profound gratitude to Professor Kusum K. Bania, Department of Chemical Sciences, Tezpur University for providing the essential laboratory facilities and for his insightful suggestions. The authors also thank SAIC-Tezpur University, SAIF-IIT Bombay, and SAIF-CSIR-NEIST, Jorhat for the instrumentation facilities.

Author contributions

MJ Baruah and R Bayan contributed to conceptualization, investigation, writing—original draft, and formal analysis. B Borthakur performed the theoretical calculations for the experiment, provided critical insights into the interpretation of the results, and elucidated the underlying mechanisms. SB Gohain, P Saikia, E Saikia, M Dey and R Kemprai contributed to investigation and writing-review, editing, investigation and visualization. YB Park contributed to investigation and writing—review & editing. B Das and M Sharma contributed to supervision, validation, and writing—review & editing.

Declarations

Competing interests

The authors declare no competing interests.

Ethical approval

The authors certify that they have no affiliations with or involvement in any organization or entity with any financial interest or non-financial interest in the subject matter or materials discussed in this manuscript.

Additional information

Supplementary Information The online version contains supplementary material available at https://doi.org/10.1038/s41598-025-92408-8.

Correspondence and requests for materials should be addressed to B.D. or M.S.

Reprints and permissions information is available at www.nature.com/reprints.

Publisher's note Springer Nature remains neutral with regard to jurisdictional claims in published maps and institutional affiliations.